ELSEVIER

Optical Materials 20 (2002) 87–96

OPTICAL Materials

www.elsevier.com/locate/optmat

Refractive index dispersion and anisotropy in Cr^{4+}:Mg_2SiO_4

Z. Burshtein [a,*], Y. Shimony [b]

[a] *Department of Materials Engineering, Ben-Gurion University of the Negev, P.O. Box 653, Beer-Sheva 84105, Israel*
[b] *Rotem Industries, Rotem industrial Park, Mishor Yamin, D.N. Arava 86800, Israel*

Received 25 May 2001; accepted 23 April 2002

Abstract

Room-temperature refractive index dispersion and anisotropy were measured in the orthorhombic Cr^{4+}:Mg_2SiO_4 (Cr^{4+}:forsterite) single crystal between 300 and 2000 nm. Use was made of bireflection in an oriented single crystal prism and of birefringence modulation in an oriented plane-parallel sample for obtaining accurate measurements of the anisotropy. Minimum-deviation measurement in an oriented prism provided the refractive index dispersion for one of the axes, whence for the other two axes as well. The crystal is biaxial, and its dielectric principal axes X, Y, and Z, coincide with the crystallographic b, a, and c axes, respectively. Taking 632.8 nm (the HeNe laser line) as a representative wavelength of the visible range, the refractive indices would be $n_a = 1.6505 \pm 0.0005$, $n_b = 1.6365 \pm 0.0006$, and $n_c = 1.6685 \pm 0.0006$. The dispersion curves were fitted to different Sellemeier functions. Our results would be very useful for the design of compensating elements of group-velocity dispersion in Cr^{4+}:Mg_2SiO_4 short-pulse laser cavities.

PACS: 78.20.Ci; 78.20.Fm; 42.70.Hj
Keywords: Refractive index; Forsterite Cr^{4+}:Mg_2SiO_4; Bireflection; Birefringence modulation; Group-velocity dispersion

1. Introduction

Since about a decade ago, forsterite, the Mg_2SiO_4 single crystal, has been extensively studied as a laser host material, especially for Cr^{4+} ions. Laser action in Cr^{4+}:Mg_2SiO_4 was demonstrated in the 1.2–1.35 μm spectral range [1–4]. Particularly, ultrashort pulses in the femtosecond range were obtained by virtue of the broad emission-band of Cr^{4+} ions in this host material [5–10]. Another potential application is as a saturable absorber for passive laser Q-switching at 1064 nm, and in the 650–750 nm spectral range [11]. Other impurity ions have also been considered for laser action, such as Ti^{3+} [12]. The refractive index dispersion and anisotropy is a fundamental physical parameter required for proper laser design and operation. Just as an example, the refractive index dispersion allows one to assess the group-velocity dispersion, an effect most important in ultrashort pulses. Quite surprisingly, this basic information for Mg_2SiO_4 is lacking in the literature. Only average refractive indices in the visible have been reported: $n_X = 1.645$, $n_Y = 1.660$, and $n_Z = 1.679$, where X, Y, and Z are the principal axes of the dielectric tensor [13]. In the present work we

* Corresponding author.
E-mail address: zeevb@bgumail.bgu.ac.il (Z. Burshtein).

0925-3467/02/$ - see front matter
PII: S0925-3467(02)00050-2

measured the room-temperature refractive index dispersion and anisotropy in Cr^{4+}:Mg_2SiO_4 in the 0.35–2.0 μm spectral range.

Forsterite is orthorhombic, and belongs to the olivine family of crystals. The lattice constants are $a = 4.762$ Å, $b = 10.225$ Å, and $c = 5.994$ Å. The unit cell contains four formula units, and the space-group is Pnma (or D_{2h}^{16} by Schönflies notation) [14]. The crystal is biaxial by virtue of symmetry, and the principal axes of the dielectric tensor coincide with the a, b, and c crystallographic orientations.

2. Method

For obtaining an initial estimate of the refractive-index anisotropy we measured the bireflection effect in an oriented single crystal prism according to a method first described by Lotem and Burshtein [15]. For completeness of presentation, we include a brief description here. The sample is prepared as a near-right-angle prism, with two of the principal dielectric axes, say, X and Z, parallel to the sides of the entrance face (Fig. 1). A non-polarized plane wave incident perpendicularly to the entrance face separates inside the prism into two X- and Z-polarized plane-wave beams, propagating according to the refractive indices n_X and n_Z, respectively. Upon internal reflection, each beam separates in two, one X-polarized, the other almost exactly Y-polarized, propagating in different directions (bireflection), in fulfillment of Snell's law: $\sin\theta = \text{const.}/n$, where θ is the angle of reflection, and n the refractive index of propagation. Thus, four reflected beams are generated, as shown in Fig. 1. The reflected beams are numbered, with subscripts indicating first the actual polarization, then the polarization of the generating component of the incident beam, both relative to the crystal principal dielectric tensor axes. For example, beam I is X-polarized, and originates from reflection of the X-polarization component of the incident beam.

In the particular case shown in Fig. 1, the reflected beams marked "II" and "III" are forbidden, as they involve a polarization change from vertical to horizontal (or vice versa). In other words, these beams should exhibit zero intensity. The beams are

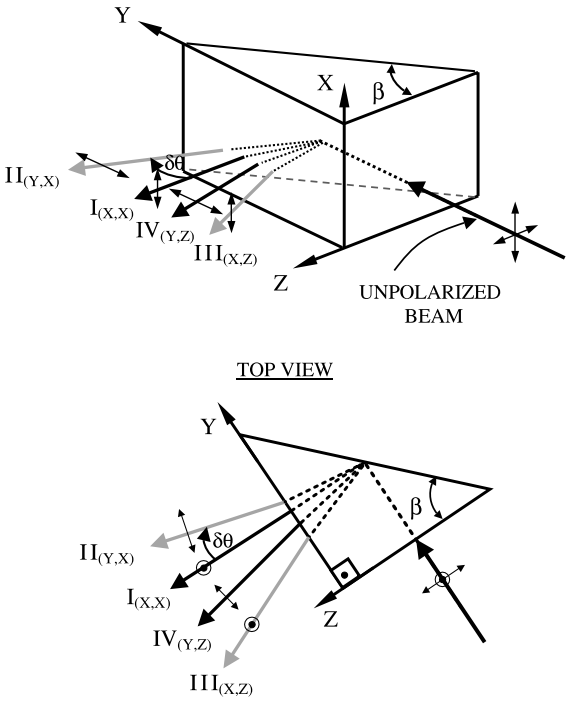

Fig. 1. Schematic view of bireflection in an oriented prism of an anisotropic material. A non-polarized beam of light splits into four polarized beams upon internal reflection.

turned on by a slight tilt of the prism, or by a minute misalignment of the principal axes, remaining however, very faint. The actual order among the different beam reflection angles is not necessarily as shown in the figure: it depends on the sign of anisotropy among the refractive indices. The identity of each beam may be unequivocally established by experiment, by using two linear polarizers, one to select the incident beam polarization, the other to analyze that of the reflected beam.

Of the four beams, only the reflection numbered "I" is specular, as the refractive indices for the incident and reflected beams are both n_X. For the other three, the change in refractive index δn manifests itself by a change in angle $\delta\theta$ relative to the specular condition. For a sufficiently small anisotropy in n, and for the apex angle β being sufficiently close to 45°, the refractive index anisotropy may be approximated by

$$\delta n \cong -\delta\theta \cot\beta + (1/n)(0.5 + \cot\beta)(\delta\theta)^2. \qquad (1)$$

Eq. (1) is readily derived by making a series expansion of Snell's Law.

A more accurate measurement of the anisotropy, which however requires support by the former one, was obtained by measuring the birefringence modulation (polarization interference) of light propagating through an oriented plane-parallel sample [16,17]. In this method, two of the crystal principal dielectric-tensor axes, for example, X and Y, lie in the sample plane, the third (Z) thus lies perpendicular to it. The optical transmission spectrum is measured when the sample is placed between crossed polarizers, each oriented at 45° between X and Y.

The experimental arrangement is shown in Fig. 2. The linearly polarized beam of light incident on the sample splits into two components, one X-polarized, the other Y-polarized, propagating at phase velocities determined by n_X and n_Y, respectively. In general, some phase change occurs between the two components. The recombined emerging light is then elliptically polarized, and some light would be transmitted through the crossed polarizer. However, at certain wavelengths λ_k, satisfying $|n_X - n_Y|_{\lambda_k} \cdot L = (j_0 + k)\lambda_k$, where L is the sample thickness, and $j_0 > 0$ and $k \geqslant 0$ are integers, the phase change between the two components is an integral multiple of 2π. The recombined outgoing light is then again linearly polarized in the original direction, and the crossed polarizer extinguishes the transmission. Thus, the transmitted light spectrum exhibits a periodic modulation, with minima at λ_k. The sum $j_0 + k$ is the birefringence order: j_0 is the transmission minimum order in the vicinity of longest measured wavelengths, and k is the count number of minima in the transmission spectrum from long to short wavelengths, starting at zero. Thus,

$$k = \frac{|n_X - n_Y|_{\lambda_k} \cdot L}{\lambda_k} - j_0. \tag{2}$$

A plot of k as a function of $|n_X - n_Y|_{\lambda_k} \cdot L/\lambda_k$ should exhibit a straight line, and yield $-j_0$ as the zero-argument intercept on the ordinate. In the experimental procedure, the anisotropy values $|n_X - n_Y|_{\lambda_k}$ are initially taken as those estimated from the bireflection (see above), and some error might be anticipated. Thus, $-j_0$ is taken as the integral number of the said intercept. Once this value is established, a calculation of the anisotropy is performed, namely $|n_X - n_Y|_{\lambda_k} = (j_0 + k)\lambda_k/L$ (Eq. (2), which provides more accurate values than those previously obtained through bireflection.

The refractive index in one of the crystallographic orientations was measured by the minimum deviation effect using the same oriented prism used for bireflection (Fig. 1). This is a long-known method: a collimated beam refracted by the prism attains a minimum deviation at an angle of incidence θ_{in} satisfying

$$\sin\theta_{\text{in}} = n \sin(\beta/2), \tag{3}$$

where β is the prism apex angle. By measuring the incidence angle at minimum deviation, the refractive index n is easily extracted. Use of these data for a particular axis, along with the anisotropy, allows one to establish the dispersion curves for all the axes.

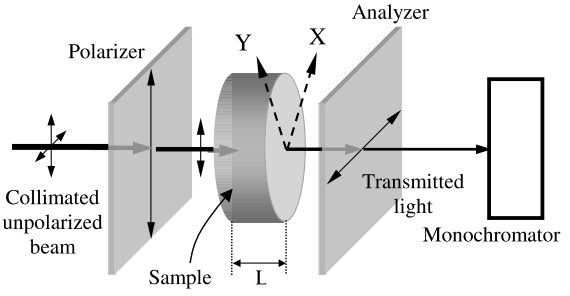

Fig. 2. Illustration of system used to measure birefringence modulation of light in a crystallographicaly oriented parallel plate. For details see text.

3. Experiment

The Cr^{4+}:Mg_2SiO_4 crystal used in the present study was self-grown [18]. The Cr^{4+} concentration was of the order of 5×10^{17} cm^{-3}. This nominal concentration of impurities should not change the refractive indices as compared to those of the pure Mg_2SiO_4. For the bireflection, as well as for the minimum-deviation measurements, a prism as in Fig. 1 was prepared, with the crystallographic a, b,

and c axes coinciding with the X, Y, Z ones of Fig. 1, respectively, and $\beta = 45°10'$. For the birefringence modulation measurements, two crystal plane-parallel plates were prepared, one 0.965 mm thick with the b and c axes in the plate plane, the other 1.272 mm thick, with the a and b axes in the plate plane. Crystallographic orientations were established by Laue X-ray back-reflection. The crystal was cut by a diamond-impregnated metallic-blade saw, and polished to high flatness and optical quality on aluminum-made flat rotating plates. Diamond-powder pastes (25 μm down to 0.3 μm particle dimension) were used as abrasive materials, and an alcohol-based suspension as the lubricant.

A variety of lasers were used as light sources for measuring the minimum-deviation and bireflection effects. A Lambda Physik type EMG-203-MSC pulsed XeCl excimer laser ($\lambda = 308$ nm); A Coherent-Innova type 100 multi-line CW argon ion laser ($\lambda = 457.5$, 476.5, 488.0, 496.5 and 514.5 nm); A Quanta-Ray type GCR-12 pulsed Nd:YAG laser in its fundamental ($\lambda = 1064$ nm), frequency-doubled ($\lambda = 532$ nm), and self-designed OPO ($\lambda = 1573$ nm); CW He–Ne lasers: Melles-Griot type SGR-871 ($\lambda = 543.0$ nm), and a Uniphase type 1125 ($\lambda = 632.8$ nm); A self designed [19] CW diode-pumped Yb:YAG laser ($\lambda = 1030$ nm). The light transmission measurements for the birefringence modulation effect were made with a JASCO UV/VIS/NIR type V-570 spectrophotometer in the 350–2000 nm spectral range.

4. Results and discussion

The measured wavelength spectra of the refractive index n_a and the anisotropies $n_c - n_b$ and $n_b - n_a$ for the laser lines used are summarized in Table 1. The measurement of $n_b - n_a$ required observation of the faint reflections (beams II and III—Fig. 1). In certain cases these beams were too faint to be observed, particularly for such wavelengths and polarizations for which considerable absorption by the Cr^{4+} ions in the Mg_2SiO_4 matrix occurred for either the reflected and/or incident light [20,21]. Thus, some data is missing in the table. The results obtained are reasonably close and quite consistent with the early visible refractive-index measurements by Sahama and Torgeson [13]. In Fig. 3 we show the dispersion curve of n_a. The data points are best fitted to a Sellemeier function of the form

$$n^2 = 1 + \frac{A\lambda^2}{B + \lambda^2 + C\lambda^{-2}}, \tag{4}$$

with $A_a = 1.5695 \pm 0.002$, $B_a = (-0.0162 \pm 0.0001)\ (\mu m)^2$, and $C_a = (5 \pm 0.4) \times 10^{-4}\ (\mu m)^4$. The existence of appreciable dispersion for both refractive-index anisotropies $(n_b - n_a)$ and $(n_c - n_b)$ is not certain. Thus, as first-order approximation for further analyses we take their averages over the measured spectral range as representatives, namely, $\overline{(n_b - n_a)} = -0.0144$, and $\overline{(n_c - n_b)} = 0.0320$.

We turn now to the birefringence modulation measurements. In Fig. 4 we show the transmission

Table 1
Refractive index n_a measured by the minimum deviation method, and the refractive-index anisotropy measured by internal bireflection in Cr^{4+}:Mg_2SiO_4

λ (nm)	n_a	$n_c - n_b$	$n_b - n_a$
308	1.696 ± 0.004	0.0307 ± 0.0005	
457.5	1.6661 ± 0.0008	0.0324 ± 0.0002	-0.0142 ± 0.0002
476.5	1.6639 ± 0.0008	0.0323 ± 0.0002	-0.0142 ± 0.0002
488.0	1.6627 ± 0.0008	0.0323 ± 0.0002	-0.0142 ± 0.0002
496.5	1.6618 ± 0.0008	0.0322 ± 0.0002	-0.0142 ± 0.0002
514.5	1.6602 ± 0.0008	0.0322 ± 0.0002	-0.0142 ± 0.0002
532	1.6596 ± 0.0008	0.0326 ± 0.0002	-0.0152 ± 0.0003
543.0	1.6555 ± 0.001	0.0327 ± 0.0002	
632.8	1.6495 ± 0.001	0.0322 ± 0.0002	
1030	1.641 ± 0.002	0.0312 ± 0.0003	
1064	1.6366 ± 0.0008	0.0318 ± 0.0001	-0.0145 ± 0.0003
1573	1.635 ± 0.010	–	

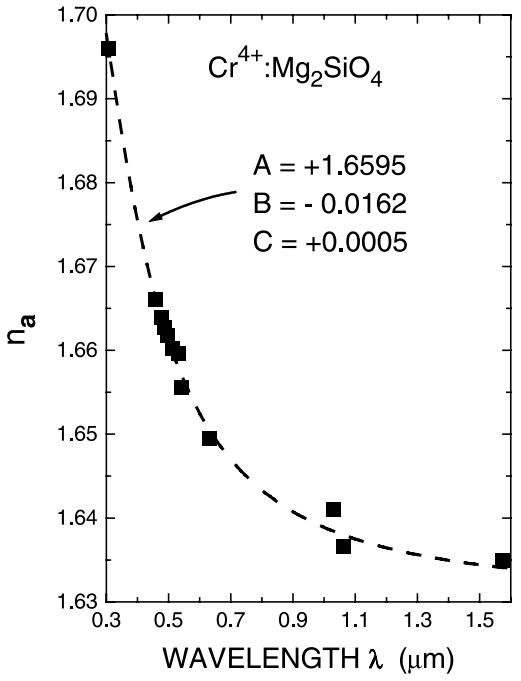

Fig. 3. Spectral dispersion of the refractive index n_a in Cr^{4+}:Mg_2SiO_4. The dashed curve indicates its fitting to a Sellemeier function of the form given in Eq. (3). The fitting parameters are indicated.

spectra through a crystal plane-parallel plate oriented in the (a, b) plane, in overlapping different spectral regions that cover the entire range between 350 and 2000 nm. The typical intensity modulation is clearly seen throughout. Some additional structure between 1600 and 1900 nm is caused by absorption structure in the plastic polarizers used (Fig. 2). In an ideal case, when the polarizers are perfectly aligned, and no absorption occurs in the sample, any transmission minimum should reach zero. In our case, the minima never reached zero, mainly because the different polarization components underwent different absorption in the sample [20,21]. This, however, has practically no effect on the wavelength positions of the minima.

In Fig. 5 we plotted the minimum count-number k as a function of $|\overline{(n_b - n_a)}| \cdot L/\lambda_k$ for the measurements shown in Fig. 4. As expected (Eq. (2)), the relation is nearly linear, with some slight curving, obviously due to dispersion in

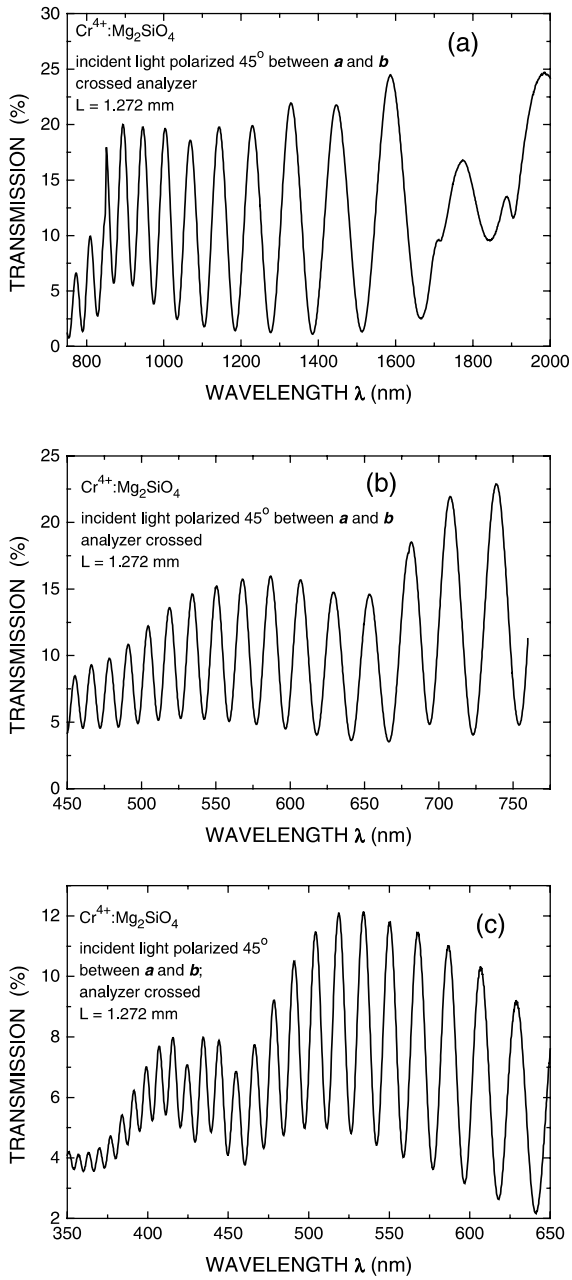

Fig. 4. Optical transmission spectra for an oriented plane-parallel plate of Cr^{4+}:Mg_2SiO_4, with the a and b crystallographic orientation in the plate plane, and placed between crossed polarizers with their easy axes at 45° between a and b. (a)–(c) are different wavelength ranges covering 350–2000 nm.

$|(n_b - n_a)|$. A linear fit sets the zero-argument intercept at $k = -10.4$. We chose, however, to

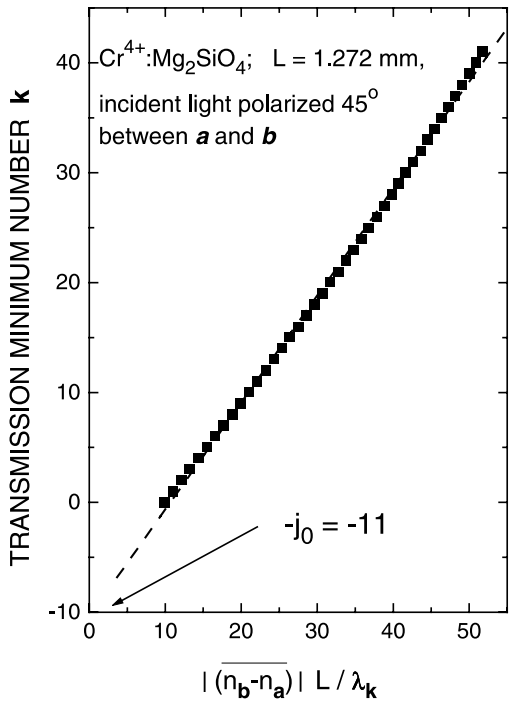

Fig. 5. Count number k of minima from long to short wavelength in Fig. 4 spectra versus $|\overline{(n_b - n_a)}| \cdot L/\lambda_k$. For details see text.

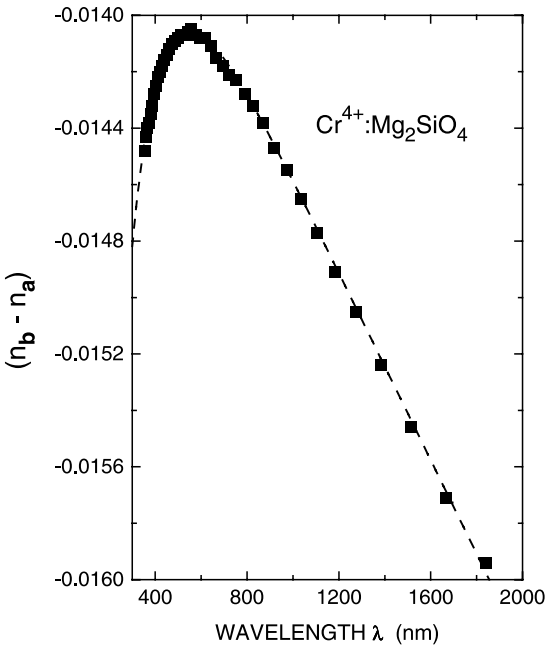

Fig. 6. Spectral dependence of the $(n_b - n_a)$ refractive-index anisotropy. Dashed line indicates fitting to an empirical function.

use the value $-j_0 = -11$ rather than $-j_0 = \mathrm{Int}(-10.4) = -10$. The reason was that a tangent line to the data near $k \approx 25$ refers to the ~500 nm region, where the average $|\overline{(n_b - n_a)}|$ was estimated. That tangent line lies slightly lower than the linear fit curve. Accordingly, $(n_b - n_a)$ was calculated as a function of wavelength using the following expression derived from Eq. (2): $(n_b - n_a)_{\lambda_k} = -(j_0 + k)\lambda_k/L$, and setting $j_0 = 11$. The minus sign on the right hand side of this expression has been previously established by the bireflection (Table 1). The results are shown in Fig. 6. The refractive-index anisotropy $(n_b - n_a)$ grows in absolute value from 0.0140 to 0.0160 between ~700 and 2000 nm, respectively. Between 350 and ~700 nm, however, $|(n_b - n_a)|$ reduces from 0.0145 to 0.0140, respectively. The dashed line in the figure is a fit of the data to an empirical function.

A similar analysis was performed for the parallel plate oriented in the (b, c) plane, yielding the $(n_c - n_b)$ refractive-index anisotropy. The results are shown in Fig. 7. The $(n_c - n_b)$ refractive-index anisotropy grows from 0.0319 to 0.0325 between ~700 and 2000 nm, respectively. Between 350 and ~700 nm, however, $(n_c - n_b)$ reduces from 0.0330 to 0.0319, respectively. The dashed line in the figure is a fit of the data to an empirical function.

Using the latter results, and the measured n_a refractive index dispersion curve (Fig. 3), the n_b and n_c dispersion curves are calculated according to $n_b = n_a + (n_b - n_a)$, then $n_c = n_b + (n_c - n_b)$. The n_a dispersion was extrapolated up to 2 μm by the same Sellemeier function (Eq. (2)). In a summary, the refractive index dispersion curves for all the dielectric principal axes are shown in Fig. 8. Both n_b and n_c are fitted to Sellemeier functions of the form

$$n^2 = 1 + \frac{\alpha\lambda^2}{\beta + \lambda^2 + \gamma\lambda^{-1.6}}, \quad \text{with} \tag{5}$$

$$\alpha_b = 1.608 \pm 0.0025,$$

$$\beta_b = (-0.0185 \pm 0.0002)\ (\mu\mathrm{m})^2,$$

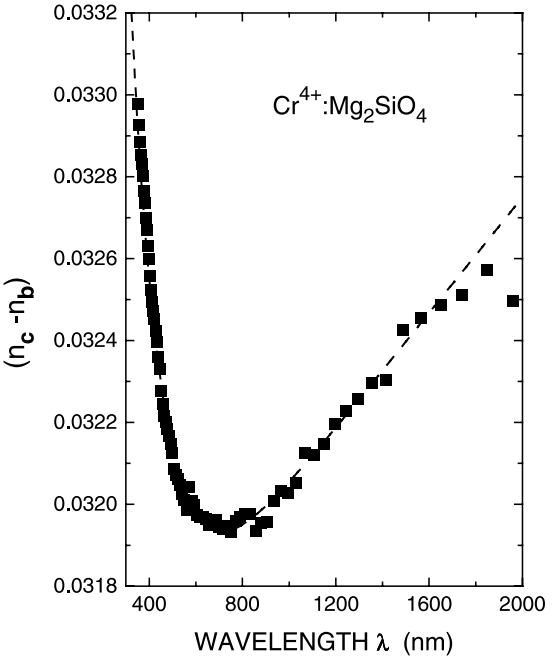

Fig. 7. Spectral dependence of the $(n_c - n_b)$ refractive-index anisotropy. Dashed line indicates fitting to an empirical function.

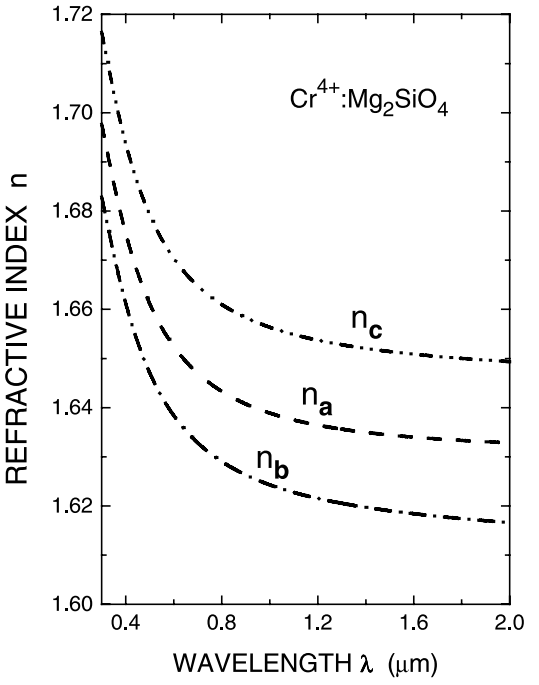

Fig. 8. Spectral dispersion of refractive indices in $Cr^{4+}:Mg_2SiO_4$ for the principal axes of the dielectric tensor. The Sellemeier functions are given in the text.

$$\gamma_b = (11.0 \pm 0.6) \times 10^{-4}\ (\mu m)^{3.6},$$

$$\alpha_c = 1.7145 \pm 0.0025,$$

$$\beta_c = (-0.0175 \pm 0.0003)\ (\mu m)^2,$$

$$\gamma_c = (9.9 \pm 0.8) \times 10^{-4}\ (\mu m)^{3.6}.$$

The main source for error stems from the error in the measuring of n_a.

Use of the dispersion curves allows a reduced estimate of error in the refractive indices at each wavelength, as compared to that specified in Table 1. For example, at 632.8 nm (the He–Ne laser line) the refractive indices would be $n_a = 1.6505 \pm 0.0005$, $n_b = 1.6365 \pm 0.0006$, and $n_c = 1.6685 \pm 0.0006$. The anisotropies $(n_b - n_a)$ and $(n_c - n_b)$ displayed in Figs. 6 and 7, respectively, are each accurate to within $\pm 5 \times 10^{-5}$ in most of the spectral range.

Some immediate conclusions follow. First, by optical convention, the principal axes of the dielectric tensor X, Y, Z are designated at an increasing order of the refractive indices. Accordingly we designate $X \| b, Y \| a$, and $Z \| c$. Second, both optic axes lie in the (b, c) plane. The angle between an optic axis and the c axis is given by [22]

$$V_c = \arcsin \sqrt{\frac{n_b^{-2} - n_a^{-2}}{n_b^{-2} - n_c^{-2}}} = \arcsin \left[\frac{n_c}{n_a} \sqrt{\frac{(n_a - n_b)}{(n_c - n_b)} \cdot \frac{(n_a + n_b)}{(n_c + n_b)}} \right]. \quad (6)$$

Due to the dispersion, the two optic axes are not unique. In Fig. 9 we plotted the wavelength variation of V_c. The variation is not large; the angle between each optic axis and c changes from approximately $(42 \pm 0.5)°$ in the visible (0.4–0.7 μm) to about $(45 \pm 0.5)°$ near 2.0 μm . The acute angle between the two optic axes $2V_c$ thus changes between $(84 \pm 1)°$ and $(90 \pm 1)°$ in the same spectral limits. Since c, the axis of highest refractive index, is also the bisectrix of $2V_c$, the Mg_2SiO_4 crystal is classified as optically positive from the visible up

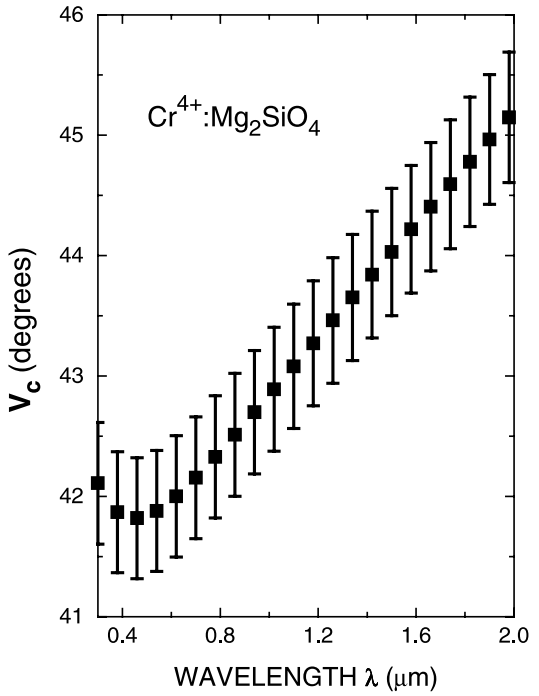

Fig. 9. Spectral change of the angle V_c between each optic axis and the c axis in Cr^{4+}:Mg_2SiO_4. Both optic axes lie in the (b, c) plane.

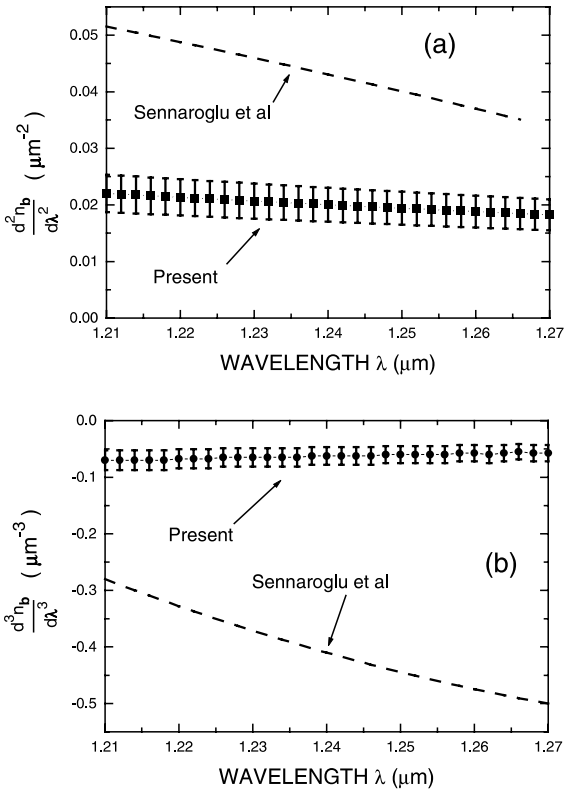

Fig. 10. Second-, and third-order wavelength derivatives of $n_b(\lambda)$ in the tuning range of a Cr^{4+}:Mg_2SiO_4 laser. Comparison is given to estimates by Sennaroglu et al. [7] based on intracavity group delay measurements of ~50-fs long pulses in a mode-locked Cr^{4+}:Mg_2SiO_4 laser.

to 2.0 μm. The same value $2V_c = 84°$ may be calculated from the early refractive-index measurements of Sahama and Torgeson in the visible [13]. Another important conclusion is the group-delay dispersion (GDD) apparent for extremely short light pulses. Due to refractive index dispersion $n(\lambda)$, the group velocity of light changes with a change in the central wavelength of the group, and the pulse time-width increases during the pulse propagation through the material. Sennaroglu et al. [7,8] measured the intracavity GDD of ~50-fs long pulses in a mode-locked Cr^{4+}:Mg_2SiO_4 laser. They used the results to assess the second-, and third-order wavelength derivatives of $n(\lambda)$ between 1.21 and 1.27 μm. In Ref. [7] they have determined $d^2n/d\lambda^2 = 0.047\ \mu m^{-2}$ and $d^3n/d\lambda^3 = -0.339\ \mu m^{-3}$ at 1.23 μm. In Ref. [8] the dispersion of each derivative is shown in the said range. In Fig. 10 we provide an estimate of the second-, and third-order wavelength derivatives of $n_b(\lambda)$ based on our results, and compare them to those of Sennaroglu et al. [8] (the b polarization direction is the one exhibiting the largest gain in Cr^{4+}:Mg_2SiO_4 [20]). Our results provide the same signs as those of Sennaroglu et al., namely, the second-order derivative is positive while the third-order one is negative. However, in our estimate, the second-order derivative is approximately half that of Sennaroglu et al., while the third-order derivative is approximately 5 times smaller in magnitude [7]. Specifically, at 1.23 μm we obtained $d^2n/d\lambda^2 = 0.0207\ \mu m^{-2}$ and $d^3n/d\lambda^3 = -0.065\ \mu m^{-3}$. Yanovsky et al. [10] obtained a GDD that is a factor of 7 smaller than that reported by Sennaroglu et al. [7]. Thus, our results seem to correspond better to the experimental results of Yanovsky et al. [10]. Our results may be used to design compensating elements for group-velocity dispersion in short-pulse laser cavities, where

Mg_2SiO_4 is the ion host matrix acting as the amplifying medium, Cr^{4+}:Mg_2SiO_4 being a first example.

5. Conclusion and summary

We provide a comprehensive room-temperature measurement of the refractive index dispersion and anisotropy of Cr^{4+}:Mg_2SiO_4 in the 300–2000 nm spectral range. Measurement of bireflection in an oriented right-angle prism of the single crystal provided an initial, somewhat rough estimate of the anisotropy. Birefringence modulation measurement in an oriented plane-parallel sample reduced the error in the determination of the refractive-index anisotropy and its dispersion. Minimum-deviation measurement in an oriented prism provided the refractive index dispersion for one of the axes, whence for the other two axes as well. The crystal is biaxial, and its dielectric principal axes X, Y, and Z, coincide with the crystallographic b, a, and c axes, respectively. n_a fits a dispersion curve of the form $n^2 = 1 + A\lambda^2/(B + \lambda^2 + C\lambda^{-2})$, with $A_a = 1.5695 \pm 0.002$, $B_a = (-0.0162 \pm 0.0001)\ (\mu m)^2$, and $C_a = (5 \pm 0.4) \times 10^{-4}\ (\mu m)^4$ in the 300–1600 nm range, and presumably up to 2000 nm. n_b and n_c fit dispersion curves of the form $n^2 = 1 + \alpha\lambda^2/(\beta + \lambda^2 + \gamma\lambda^{-2.6})$, with $\alpha_b = 1.608 \pm 0.0025$, $\beta_b = (-0.0185 \pm 0.0002)\ (\mu m)^2$, and $\gamma_b = (11.0 \pm 0.6) \times 10^{-4}\ (\mu m)^{3.6}$; $\alpha_c = 1.7145 \pm 0.0025$, $\beta_c = (-0.0175 \pm 0.0003)\ (\mu m)^2$, and $\gamma_c = (9.9 \pm 0.8) \times 10^{-4}\ (\mu m)^{3.6}$. Taking 632.8 nm (the HeNe laser line) as a representative wavelength in the visible, the refractive indices would be $n_a = 1.6505 \pm 0.0005$, $n_b = 1.6365 \pm 0.0006$, and $n_c = 1.6685 \pm 0.0006$. Our results would be very useful for the design of compensating elements for group-velocity dispersion in Cr^{4+}:Mg_2SiO_4 short-pulse-laser cavities.

Acknowledgements

We are indebted to Dr. A. Sennaroglu for pointing out to us the need for carrying out a detailed measurement of refractive index dispersion in Cr^{4+}:Mg_2SiO_4. The technical assistance of Mr. L. Kravchyk is greatly appreciated.

References

[1] V. Petricevic, S.K. Gayen, R.R. Alfano, K. Yamagishi, H. Anzai, Y. Yamaguchi, Laser action in chromium-doped forsterite, Appl. Phys. Lett. 52 (1988) 1040.
[2] V. Petricevic, S.K. Gayen, R.R. Alfano, Continuous-wave laser operation of chromium-doped forsterite, Opt. Lett. 14 (1989) 612.
[3] T.J. Carrig, C.R. Pollock, Tunable, CW operation of a multiwatt forsterite laser, Opt. Lett. 16 (1991) 1662.
[4] H.R. Verdun, L.M. Thomas, D.M. Andrauskas, T. McCollum, A. Pinto, Chromium-doped forsterite laser pumped with 1.06 m radiation, Appl. Phys. Lett. 53 (1988) 2593.
[5] A. Sennaroglu, T.J. Carrig, C.R. Pollock, Femtosecond pulse generation by using an additive-pulse mode locked chromium-doped forsterite laser operated at 77 K, Opt. Lett. 17 (1992) 1216.
[6] A. Seas, V. Petricevic, R.R. Alfano, Generation of sub-100-fs pulses from a CW mode-locked chromium-doped forsterite laser, Opt. Lett. 13 (1992) 937.
[7] A. Sennaroglu, C.R. Pollock, H. Nathel, Generation of 48-fs pulses and measurement of crystal dispersion by using a regeneratively initiated self-mode-locked chromium-doped forsterite laser, Opt. Lett. 18 (1993) 826.
[8] A. Sennaroglu, C.R. Pollock, H. Nathel, Generation of tunable femtosecond pulses in the 1.21–1.27 and 605–635 μm wavelength region by using a regeneratively initiated self-mode-locked Cr:forsterite laser, IEEE J. Quantum Electron. 30 (1994) 1851.
[9] Y.P. Tong, P.M.W. French, J.R. Taylor, J.O. Fujimoto, All-solid-state femtosecond sources in the near infrared, Opt. Comm. 136 (1997) 235.
[10] V. Yanovsky, Y. Pang, F. Wise, B.I. Minkov, Generation of 25-fs pulses from a self-mode-locked Cr:forsterite laser with optimized group-delay dispersion, Opt. Lett. 18 (1993) 1541.
[11] B. Lipavsky, Y. Kalisky, Z. Burshtein, Y. Shimony, S. Rotman, Some optical properties of Cr^{4+}-doped crystals, Opt. Mater. 13 (1999) 117.
[12] L. Shenjun, L. Lin, J. Yanado, J. Xiaobo, W. Xing, Growth and characteristics of Mg_2SiO_4:Ti, J. Cryst. Growth 139 (1994) 327;
J. Cryst. Growth 53 (1988) 2593.
[13] Th.G. Sahama, D.R. Torgeson, Thermochemical study of the olivines and orthopyroxenes, US Bur. Mines Rept. Invest. 4408, 1949.
[14] J.D. Birle, G.V. Gibbs, P.B. Moore, J.V. Smith, Crystal structure of natural olivines, Amer. Mineral. 53 (1968) 807.
[15] H. Lotem, Z. Burshtein, Method for complete determination of the refractive index tensor by bireflectance: Application to $CdWO_4$, Opt. Lett. 12 (1987) 561.
[16] R.W. Ditchburn, Light, Interscience, New York, 1963, Chapter 12.

[17] T.S. Moss, Optical properties of semiconductors, Butterworth, London, 1961.
[18] See e.g., Y. Shimony, Cr^{4+}-doped crystals for laser applications, in: M. Oron, I. Shladov, Y. Weissman (Eds.), Proceedings of the 8th meeting on optical engineering in Israel, December 1992, SPIE vol., 1972, p. 139.
[19] Y. Kalisky, C. Labbé, K. Waichman, L. Kravchik, U. Rachum, P. Deng, J. Xu, J. Dong, W. Chen, Passively Q-switched, diode-pumped Yb:YAG using Cr^{4+}-doped garnets, Opt. Mater., in press.
[20] N.V. Kuleshov, V.G. Shcherbitsky, V.P. Mikhailov, S. Hartung, T. Danger, S. Kück, K. Petermann, G. Huber, Excited state absorption and stimulated emission measurements in Cr^4:forsterite, J. Lumin. 75 (1997) 319.
[21] N.V. Kuleshov, V.G. Scherbitsky, V.P. Mikhailov, S. Hartung, S. Kück, K. Petermann, G. Huber, Near infrared and visible excited-state absorption in Cr^4:forsterite, in: R.P. Clifford, R.B. Walter (Eds.), OSA Trends in Optics and Photonics vol. 10, Advanced Solid State Lasers, Optical Society of America, Washington DC, 1997, p. 425.
[22] See e.g. V.G. Dmitriev, G.G. Gurzadyan, D.N. Nikogosyan, Handbook of Non-linear Crystals, 3rd ed., Springer, Berlin, 1999, p. 17.